Improving the Strength of ZTA Foams with Different Strategies: Immersion Infiltration and Recoating

**Xiaodong Chen [1],*, Ulf Betke [2], Stefan Rannabauer [1] , Paul Clemens Peters [1],
Gerrit Maximilian Söffker [1] and Michael Scheffler [1]**

[1] Department of Mechanical Engineering, Institute for Materials and Joining Technology,
    Otto-von-Guericke-University Magdeburg, Große Steinernetischstraße 6, 39104 Magdeburg, Germany;
    stefan.rannabauer@ovgu.de (S.R.); paul.peters@st.ovgu.de (P.C.P.);
    gerrit-maximilian.soeffker@st.ovgu.de (G.M.S.); m.scheffler@ovgu.de (M.S.)
[2] Chemical Institute—Industrial Chemistry, Otto-von-Guericke-University Magdeburg, Universitätsplatz 2,
    39106 Magdeburg, Germany; ulf.betke@ovgu.de
*   Correspondence: xiaodong.chen@ovgu.de; Tel.: +49-391-67-54557

Abstract: The combination of high strength and toughness, excellent wear resistance and moderate density makes zirconia-toughened alumina (ZTA) a favorable ceramic, and the foam version of it may also exhibit excellent properties. Here, ZTA foams were prepared by the polymer sponge replication method. We developed an immersion infiltration approach with simple equipment and operations to fill the hollow struts in as-prepared ZTA foams, and also adopted a multiple recoating method (up to four cycles) to strengthen them. The solid load of the slurry imposed a significant influence on the properties of the ZTA foams. Immersion infiltration gave ZTA foams an improvement of 1.5 MPa in compressive strength to 2.6 MPa at 87% porosity, only resulting in a moderate reduction of porosity (2–3%). The Weibull modulus of the infiltrated foams was in the range of 6–9. The recoating method generated an increase in compression strength to 3.3–11.4 MPa with the reduced porosity of 58–83%. The recoating cycle dependency of porosity and compression strength is nearly linear. The immersion infiltration strategy is comparable to the industrially-established recoating method and can be applied to other reticulated porous ceramics (RPCs).

Keywords: ZTA foams; infiltration; recoating; compression strength; Weibull modulus

1. Introduction

Ceramic foams offer low density, high corrosion resistance, high permeability, high surface area, and low thermal conductivity, and due to their unique properties they have found a wide range of applications, such as filters for molten metals and hot gases, catalyst supports, heat exchangers, and porous implants [1–4]. Zirconia-toughened alumina (ZTA) composite ceramics have been investigated for several decades and exhibit high flexural strength (as high as 1000 MPa), high toughness (even > 10 MPa·m$^{0.5}$), excellent wear resistance, and biocompatibility [5–8]. They have been commercialized in biomedical implants or cutting tools and still attract wide attention [9–13]. However, most of the studies were focused on the dense form of ZTA ceramics and less of them deal with cellular ZTA ceramics. It is, therefore, necessary to study and develop ZTA foams to extend their applications.

The polymer replica method developed by Schwartzwalder and Somers [14] is one of the most common approaches to fabricate reticulated porous ceramics. It involves the coating of polymer sponges with a ceramic slurry, drying, burning out the polymer templates at moderate temperatures, and finally sintering to densify the ceramic. RPCs fabricated by this method are of lower density, higher pore connectivity, and lower pressure drop compared to the ones from the methods of direct foaming and sacrificial templates. However, as a result of the oxidation of the polymer sponge templates,

hollow struts within the reticulated ceramic body are left, which significantly degrades the strength and stability of these ceramic foams. This problem must be addressed to guarantee their reliability in practical applications.

To date, several strategies have been adapted to enhance the strength of RPCs, such as vacuum infiltration [15–18], recoating [19–25], fiber or whisker reinforcement [26–30], pre-treating of the polymeric sponge [31–33], modification of the slurry with additives [34,35], or slurry vacuum degassing [36]. Among these methods, vacuum infiltration has been proved to be an effective method to fill the hollow struts and, thus, to improve the strength of RPCs, while decreasing the total porosity only to a low extent [18]. Vogt et al. enhanced the compression strength of ZTA foams by vacuum infiltration to almost 400%, reducing the total porosity by only 1% [15]. Multi-layered dense struts were manufactured by infiltrating reticulated SiC foams with an alumina slurry under reduced pressure [16] and demonstrated a significant improvement in compressive strength and thermal shock resistance. However, an obvious drawback is that vacuum infiltration requires more complex equipment and operations, so it is hardly suitable for large batch treatments.

Here, the infiltration approach is proposed, whereby the hollow struts of the RPCs are filled by immersion without demanding vacuum conditions. This method is based on the strut cracks which are penetrated by the infiltration slurry in order to fill the hollow strut cavities. In general, such cracks are generated by the thermal stress resulting from expansion differences between the polymer template and the coating [37]. It is expected that a ceramic slurry with a suitable flow behavior and particle size could penetrate the hollow struts through cracks just by immersing RPCs into a suspension and dwelling for a certain period of time (immersion infiltration). For this process, the size of the ceramic particles in the slurry is a critical parameter. If the particle size is too large, they block the openings of the strut material cracks and no, or only a partial, filling of the struts is possible. The other important factor for the process is the viscosity of the infiltration slurry. A low viscosity, which is found for slurries with low solid load, can guarantee the strut infiltration, but after drying and sintering, not enough material is left to fill the hollow struts; on the contrary, slurries with higher solid load exhibit higher viscosity and are more difficult to infiltrate into the struts.

Therefore, in the present work a ceramic powder with fine particle size (200–300 nm) is applied to prepare a ceramic suspension with a different solid load. By varying the solid load and the concentration of additive agents (deflocculant, binder) the proper viscosity of the slurry for the immersion infiltration is adjusted. ZTA foams, prepared by the polymer sponge replica method, are the base materials to be processed and characterized before and after the immersion infiltration. They are compared with respect to density, porosity, compressive strength, Weibull modulus, and their microstructure. In addition to infiltration, especially in industrial practice, recoating is one of the most common strengthening methods for RPCs by thickening the struts and filling surface cracks and defects. For comparison, this technique is also employed and the influence of the number of recoating cycles on the properties of ZTA foams is investigated.

2. Experimental Details

2.1. ZTA Foam Preparation

The foams were prepared by the sponge replica method (Schwarzwalder process). Polyurehtane (PU) sponges (20 ppi (pores per inch), 15 × 15 × 20 mm, KoeppSchaum GmbH, Oestrich-Winkel, Germany) were used as polymer templates. As ceramic starting materials, commercial ZTA powders with a particle size of 200–300 nm and 16 wt % or 20 wt % stabilized ZrO_2 (3 wt % Y_2O_3) were employed (ZTA16, 4.19 g/cm^3, specific surface area 12.7 m^2/g; and ZTA20, 4.26 g/cm^3, specific surface area 13.2 m^2/g, TAIMICRON, Taimei Chemicals, Tokyo, Japan).

The first step was to prepare the ZTA slurries as outlined in Figure 1. An ethanolammonium citrate based deflocculant (Dolapix CE 64, Zschimmer and Schwarz Chemie GmbH, Lahnstein, Germany) was dissolved in deionized water and ZTA powder added to the solution. After mixing for 15 min at

1500 rpm in a planetary centrifugal mixer (THINKY Mixer ARE-250, THINKY Corp., Tokyo, Japan) a polyvinylalcohol-based binder (Optapix PA 4G, Zschimmer and Schwarz Chemie, GmbH, Lahnstein, Germany) and a nonionic alkyl polyalkylene glycolether-based anti-foaming agent (Contraspum K1012, Zschimmer and Schwarz Chemie GmbH, Lahnstein, Germany) were added and the suspension mixed for 30 min at 1500 rpm. ZTA slurries with solid loads of 70 wt % and 80 wt % were prepared by adjusting the content of ZTA powder. The weight ratios of deflocculant, binder, and anti-foaming agent correspond to 1.0 wt %, 1.5 wt %, and 0.1 wt % of the mass of the ZTA powder.
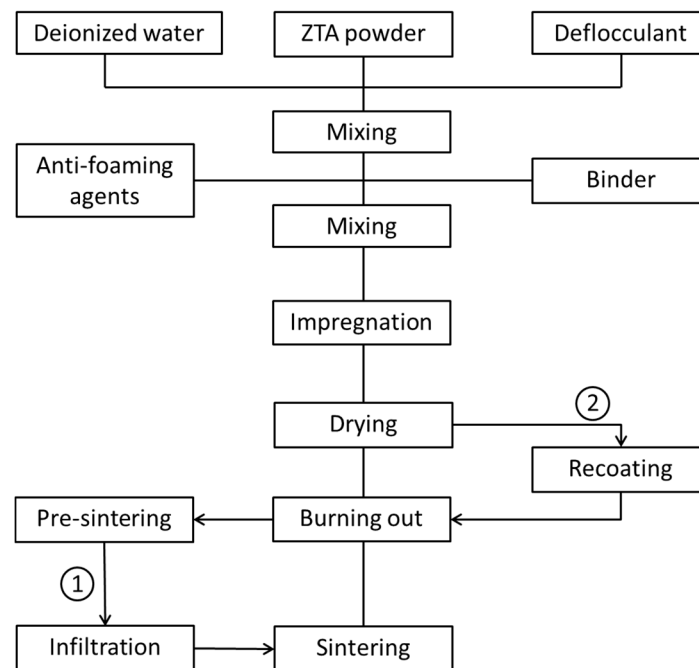

Figure 1. Flowchart of the experimental procedures for preparing and strengthening ZTA foams.

PU foams were fully impregnated with the ZTA slurry by manual and repeated compressing in the suspension. Afterwards the excess slurry in the PU foams was squeezed out, resulting in a thin slurry coating on the strut surface. To improve the pore interconnectivity of the final products, blocked pores in the coated bodies were carefully opened by compressed air blowing and the coated foams dried under ambient conditions for 24 h. The green-bodies were placed into an air furnace (KU 40/04/A, THERMCONCEPT Dr. Fischer GmbH, Bremen, Germany) to oxidize the PU templates by a three-step heating program (110 °C, 2 h; 250 °C, 3 h; 400 °C, 3 h) with a low heating rate of 1 K/min. Then they were transferred to a sintering furnace (HTL 10/17, THERMCONCEPT Dr. Fischer GmbH, Bremen, Germany). The remaining organics were oxidized in air at 600 °C for 3 h and then sintered at 1650 °C for 3 h. The heating and cooling rate were both set to 3 K/min.

Four series of ZTA foams were generated and referred to as ZTA16-70, ZTA16-80, ZTA20-70, and ZTA20-80, where the last two digits indicate the respective solid load of the slurry.

2.2. Immersion Infiltration of ZTA Foams

The foams to be infiltrated were fabricated with ZTA20 powder and partially sintered at 1200 °C to obtain the appropriate mechanical strength so that they can withstand the following operations (routine 1 in Figure 1). The preparation of the infiltration slurry was quite similar to the one as described in the previous section. The solid load with ZTA20 (particle size of 200–300 nm) of the slurry was adjusted to 50 wt % or 60 wt %, respectively. In contrast to the coating slurry no binder was added to obtain a lower viscosity. The pre-sintered foams were immersed into the slurry, dwelling for 10 min or 60 min to allow the slurry to flow into the hollow struts. The effect of the dwelling time

on the infiltration results was investigated. After the infiltration, the foams were removed from the slurry and carefully blown out with compressed air to remove the excess slurry blocking pores and adhering to the struts. After drying at ambient conditions for 24 h, they were sintered at 1650 °C for 3 h comparable to the ZTA20 foams. Based on the different solid load of the infiltration suspensions and dwelling time, the infiltrated foams were classified as ZTA20-50-10, ZTA20-50-60, ZTA20-60-10, ZTA20-50-60, where the last two digits represent the dwelling time and the two digits before are the ZTA solid load of the infiltration slurry.

2.3. Recoating of ZTA Foams

Dry green bodies of ZTA20-80 were recoated with a slurry containing 60 wt % ZTA20 (routine 2 in Figure 1). The slurry preparation was in accordance with Section 2.1. The green bodies were immersed in the recoating slurry, soaked for a few seconds, and removed from the slurry. Excess slurry blocking pores was blown out carefully with compressed air. After drying at ambient conditions for 24 h the recoated green bodies were thermally treated in accordance with Section 2.1. In order to study the influence of the number of recoating cycles, one, two, and four cycles were performed. The corresponding final foams are referred to ZTA20-R1, ZTA20-R2, and ZTA20-R4, respectively.

2.4. Characterization

The relative density of the ZTA foams was calculated from the theoretical density of the strut materials and the (total) porosity was deduced. Isotropic shrinkage was observed and the linear shrinkage was calculated by the change of the largest edge length of the foams. The macrostructure of the foams was characterized by μ-computed tomography with a Phoenix Nanotom S and software package dataos|x V2.0 (μ-CT; GE Sensing and Inspection Technologies GmbH, Wunstorf, Germany). The μ-CT reconstructions were visualized with myVGL V2.1 (Volume Graphics GmbH, Heidelberg, Germany) and structural calculations were performed with CTAnalyser (CTAn V1.16, Skyscan/Bruker microCT, Kontich, Belgium) after segmentation. Segmentation in air and material was performed by using global thresholding, whereby the gray value was deduced from the histogram. For the calculation of the strut thickness, a closing operation was applied to close the hollow struts. The compositions of ZTA foams were identified by X-ray diffraction (XRD; PANalytical GmbH, Kassel, Germany) with Cu-Kα radiation. The microstructure was observed by scanning electron microscopy (SEM; XL30 ESEM-FEG, FEI/Philips, Hillsboro, OR, USA). The compression tests for ZTA foams were performed on a uni-axial testing machine (TIRAtest 2825, Tira-GmbH, Schalkau, Germany), and the displacement, load and time were recorded. The loading rate was set to 1 mm/min, and 10 specimens were used for each test. A two-parameter Weibull distribution was applied to analyze the compression strength variability, and the Weibull modulus m was obtained by linear regression.

3. Results and Discussion

3.1. The Original ZTA Foams

Figure 2 represents the macrostructure of the foams ZTA16-70 and ZTA20-80, both showing a relatively uniform structure without obviously-blocked pores. This indicates that the process route is appropriate for the manufacturing of uniform ZTA foams. However, the solid load of the slurry greatly affects the strut thickness and integrity of the RPCs. In ZTA16-70, the struts are quite thin and fragile with a mean strut thickness of 0.49 mm while, in ZTA16-80, the mean strut thickness is 0.56 mm. Many longitudinal strut cracks can be observed inside ZTA16-70, but they are less prominent on the strut surface of the ZTA20-80. In principal, this can be explained by the rheological behavior of the coating slurries as discussed elsewhere [38].
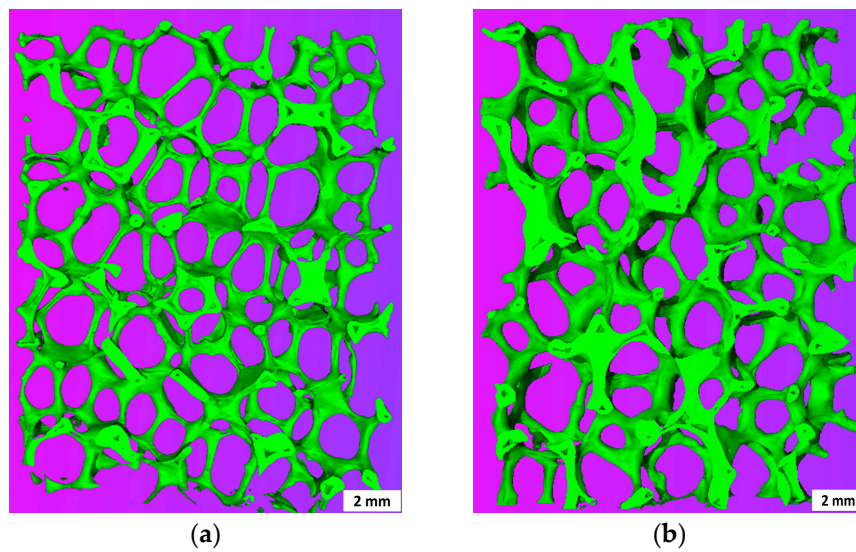
Figure 2. μ-CT 3D reconstruction of 3 mm thick slices of (**a**) ZTA16-70 and (**b**) ZTA20-80.

The microstructure and strut surface of ZTA foams were observed by SEM, as shown in Figure 3. The dark (gray) grains in Figure 3a–c, represent the alumina matrix and the bright (white) grains represent the zirconia reinforcement particles. The zirconia is homogenously distributed in the alumina matrix, preventing abnormal grain growth [39,40]. Despite the relatively high sintering temperature, the grain size of alumina ranges about 1–2 μm, and the zirconia grain size is still in the submicron scale. Figure 3d shows the existence of the typical hollow struts in ZTA foams. The strut surface is quite smooth without micro-cracks, but longitudinal cracking of the strut wall can be observed at vertices of hollow struts, as already discussed. The immersion infiltration method is based on such cracks.

The phase composition of ZTA foams was also studied by the XRD technique, as demonstrated in Figure 4. In accordance with the SEM observations, the main phases are corundum and zirconia. The zirconia consisted of tetragonal ZrO_2 and a small amount of monoclinic ZrO_2.
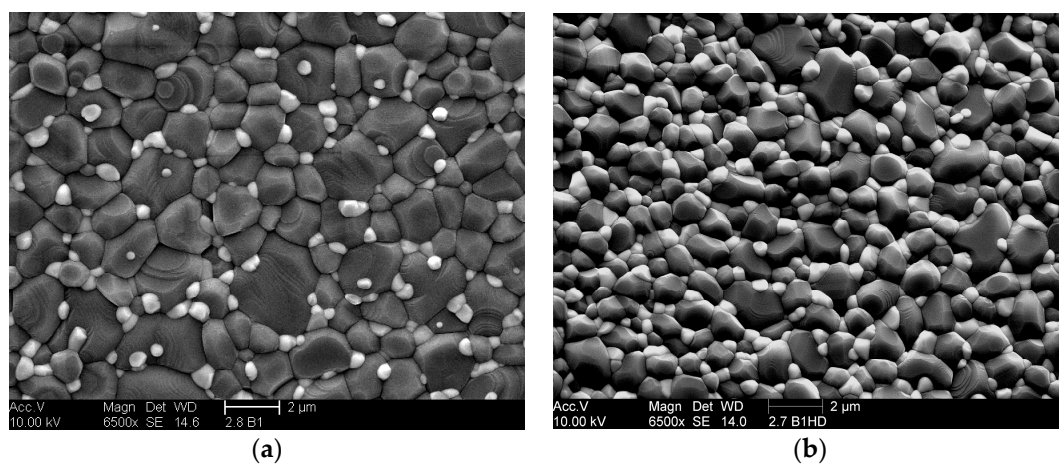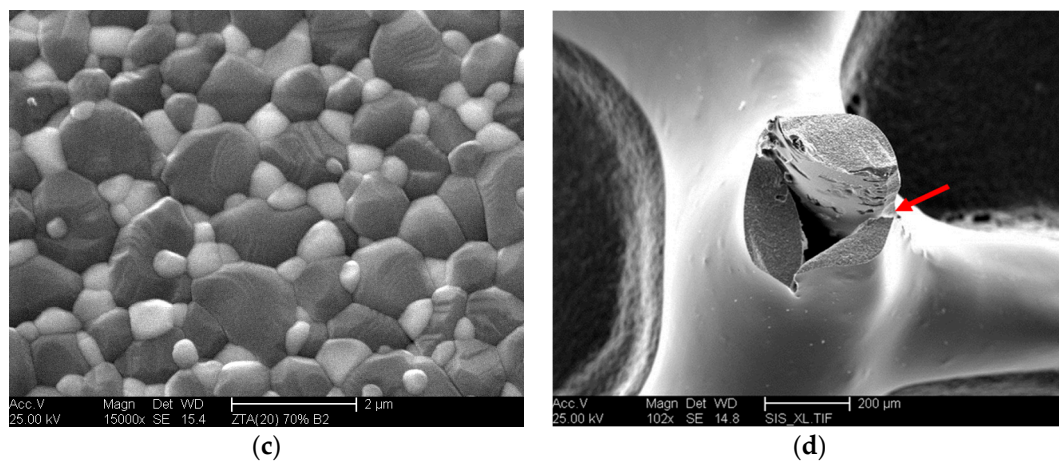

Figure 3. *Cont.*

Figure 3. SEM images of ZTA foams: (**a**) strut surface of ZTA16-80, white and gray grains are ZrO_2 and Al_2O_3, respectively; (**b**) strut surface of ZTA20-80; (**c**) higher magnification image of a strut face of ZTA20-70; and (**d**) strut structure of ZTA16-80.
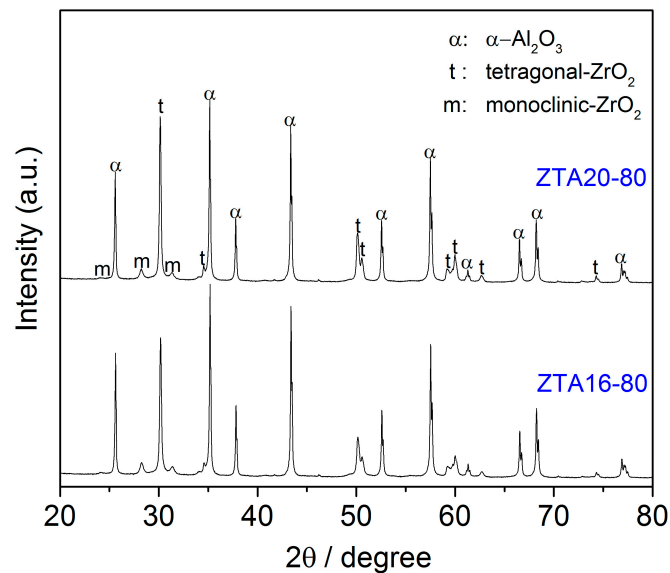

Figure 4. XRD diffraction patterns for ZTA16-80 and ZTA20-80.

Figure 5 shows the comparison of density and porosity in ZTA foams. There is no obvious influence of the ZrO_2 content on the density and porosity of the ZTA foams, while the solid load imposes a significant influence on this. ZTA16-70 and ZTA20-70 have a high porosity of 94% (density about 0.26 g/cm^3). In contrast, their counterparts ZTAxx-80 reach almost two-fold in density and about 90% in porosity.

The linear shrinkage of ZTA foams was also investigated, as listed in Table 1. The solid load of the ceramic suspension also affects the shrinkage behavior of ZTA foams. The ZTAxx-70 series has 15.5% linear shrinkage, while ZTAxx-80 exhibits only 12.6%.
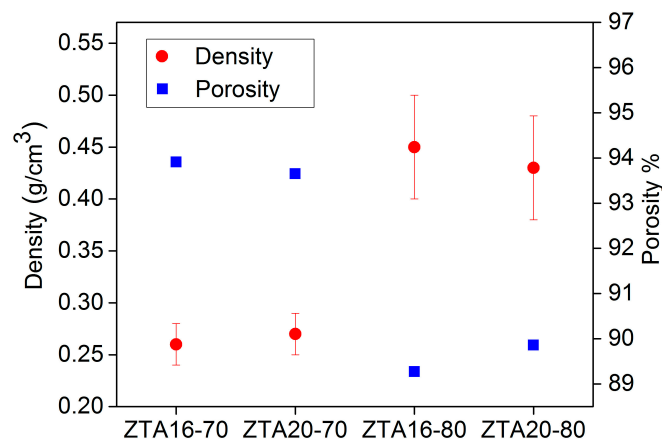
Figure 5. Density and porosity comparison for original, uninfiltrated ZTA foams.

Table 1. The properties of the original ZTA foams, infiltrated and recoated foams, with respect to density, porosity, mean strut thickness, weight gain, compression strength, Weibull modulus, and linear shrinkage.

Foams	Density [g·cm^{-3}]	Porosity [%]	Mean Strut Thickness [mm]	Weight Gain [%]	Compression Strength [MPa]	Weibull Modulus	Linear Shrinkage [%]
The first coating step							
ZTA16-70	0.26 ± 0.02	93.9	0.49 ± 0.19	—	0.08 ± 0.01	9.47	15.55
ZTA16-80	0.45 ± 0.05	89.3	0.56 ± 0.17	—	0.91 ± 0.40	8.48	12.62
ZTA20-70	0.27 ± 0.02	93.7	—	—	0.14 ± 0.02	2.30	15.38
ZTA20-80	0.43 ± 0.05	89.9	—	—	1.06 ± 0.30	4.23	12.63
The immersion infiltration step							
ZTA20-50-10	0.56 ± 0.05	86.8	0.57 ± 0.18	20.31 ± 6.11	2.20 ± 0.33	9.04	—
ZTA20-50-60	0.54 ± 0.03	87.3	0.55 ± 0.16	14.10 ± 4.37	2.55 ± 0.41	7.69	—
ZTA20-60-10	0.55 ± 0.02	87.1	0.56 ± 0.16	16.19 ± 5.12	2.09 ± 0.29	9.08	—
ZTA20-60-60	0.59 ± 0.02	86.3	0.55 ± 0.17	20.81 ± 7.17	2.66 ± 0.33	6.26	—
The recoating step							
ZTA20-R1	0.74 ± 0.05	82.4	0.82 ± 0.23	49.74 ±15.05	3.26 ± 0.71	4.04	—
ZTA20-R2	1.11 ± 0.07	73.6	0.95 ± 0.28	127.16 ±18.02	5.61 ± 0.87	7.62	—
ZTA20-R4	1.74 ± 0.08	58.5	1.41 ± 0.45	250.91 ± 28.41	11.44 ± 1.44	8.80	—

The compression strength of ZTA foams was identified with uni-axial compression tests, and their compression behavior was investigated. According to Gibson and Ashby [1], the relative density is the most important characteristic for cellular solids, and the mechanical properties greatly depend on it. As mentioned above, the solid load of the ceramic suspensions made a significant difference on the density and the porosity of the ZTA foams, thus, the solid load influences the compression strength. Figure 6 shows the results for ZTA foams. The compression strength of the foams with 10% relative density (80 wt % solid load) is almost 10 times that of the 6% relative density foams (70 wt % solid load), reaching more than 1 MPa (ZTA20-80). This can be attributed to the differences in strut thickness and the strut integrity discussed in Section 3.1. The longitudinal cracks occurring inside the struts, deteriorate the mechanical properties of ZTA foams [41,42]. For the effect of ZrO_2 content on the strength of ZTA foams, with the increase of the ZrO_2 content in the Al_2O_3 matrix from 16 wt % to 20 wt %, only a slight improvement in compressive strength of ZTA foams was observed.
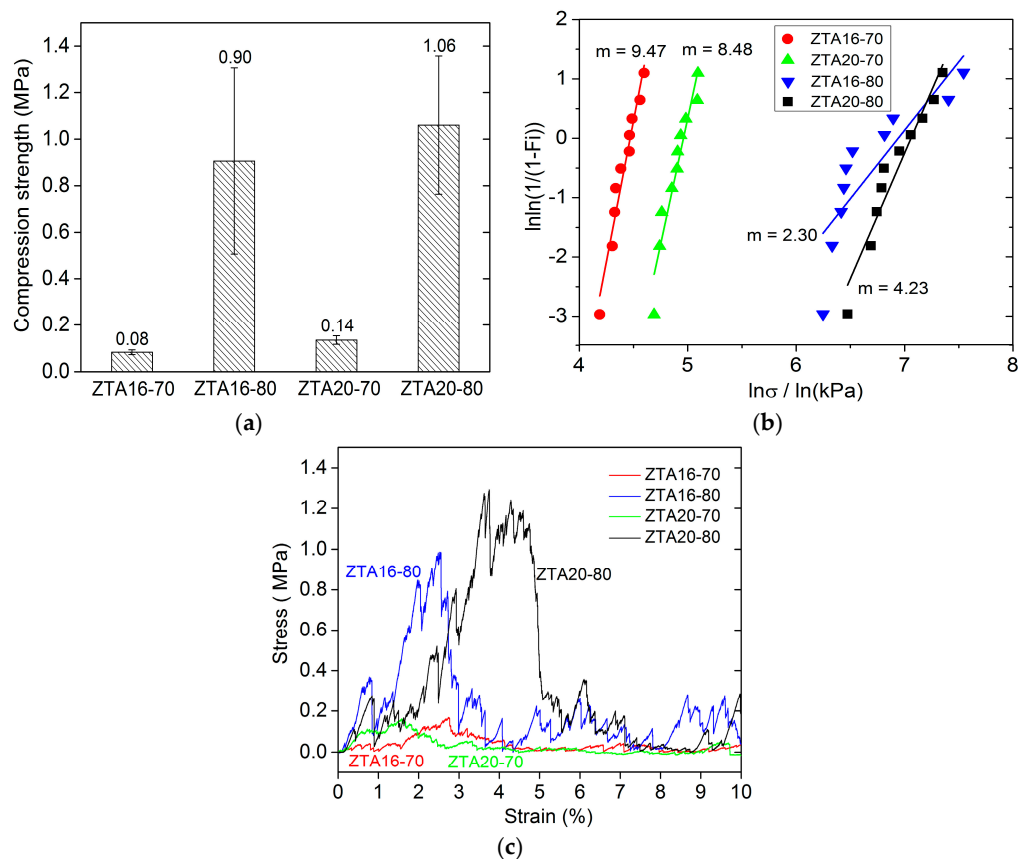
Figure 6. Compression tests for ZTA foams: (**a**) compression strength for ZTA foams; (**b**) Weibull distribution plots of original ZTA foams and (**c**) the comparison of exemplary stress/strain curves obtained from different foams.

Figure 6b presents the Weibull distribution of compression strength of ZTA foams. Noteworthy, for the foams from 70 wt % solid load, though they possess extremely low compression strength, but their compression values demonstrate quite a narrow scattering. The Weibull moduli of ZTA16-70 and ZTA20-70 are up to 9.47 and 8.48, respectively. By contrast, the compressive values of foams from 80 wt % solid load scatters in a wide range, indicating the relatively large variability of compression strength, especially for the ZTA16-80 foams, of which the Weibull modulus is only 2.30. The mechanical stability of the foams is also associated with the triangular voids in the struts, which leads to stress concentration at the sharp edges. However, for the high Weibull modulus of foams from the 70 wt % solid load, it cannot be well explained. For the compression tests, the compression load and strain were recorded, as shown in Figure 6c. The stress/strain curves indicate that ZTA foams also behave like typical ceramic foams in which, firstly, some weak struts were broken corresponding to the low peaks before the compression plateau. Afterwards, the foams experienced a compression platform, reaching their crushing point, followed by a complete failure corresponding to a sharp stress drop in compressive curves. However, an interesting difference between foams can be observed. ZTA20-80 experiences a shifting of the compression plateau compared to ZTA16-80. The shifting of the compression plateau indicates a higher stability or toughness for the higher ZrO_2 content.

3.2. Improving the Strength of ZTA Foams by Immersion Infiltration

The starting foams for immersion infiltration were ZTA20-80 foams pre-sintered at 1200 °C for 3 h; by the μ-CT imaging technique, strut cracks could be identified, as the red arrows indicate in Figure 7a. Figure 7b–e demonstrates the cross-section images from μ-CT 3D reconstructions for ZTA

foams after immersion infiltration treatments. The amount of hollow struts is substantially reduced, though some of them are incompletely filled or still empty. Especially, the connections between the vertices are blocked by solid material. Therefore, it can be concluded that the immersion infiltration is a successful strategy to reduce or eliminate triangular voids in the struts of ceramic foams. The reason for incompletely filled struts can be attributed to the lack of cracks and/or to small gaps of some cracks, so the slurry cannot penetrate their hollow voids directly and must flow from the neighboring struts. As the slurry infiltrates from different directions, an air-tight chamber can be generated in these hollow struts, preventing the further infiltration of the slurry due to the inside air pressure. As a result, these struts were just partly filled or even still empty.

The slurry of 60 wt % solid load (Figure 7d,e) has the slightly better infiltration effect than the one of 50 wt % (Figure 7b,c), resulting in fewer voids. By extending the dwelling time from 10 min (Figure 7b,d) to 60 min (Figure 7c,e), no significant differences can be observed. This implies that the flow of the ceramic suspension was fast enough to achieve the balance between outside liquid pressure and inside air pressure.
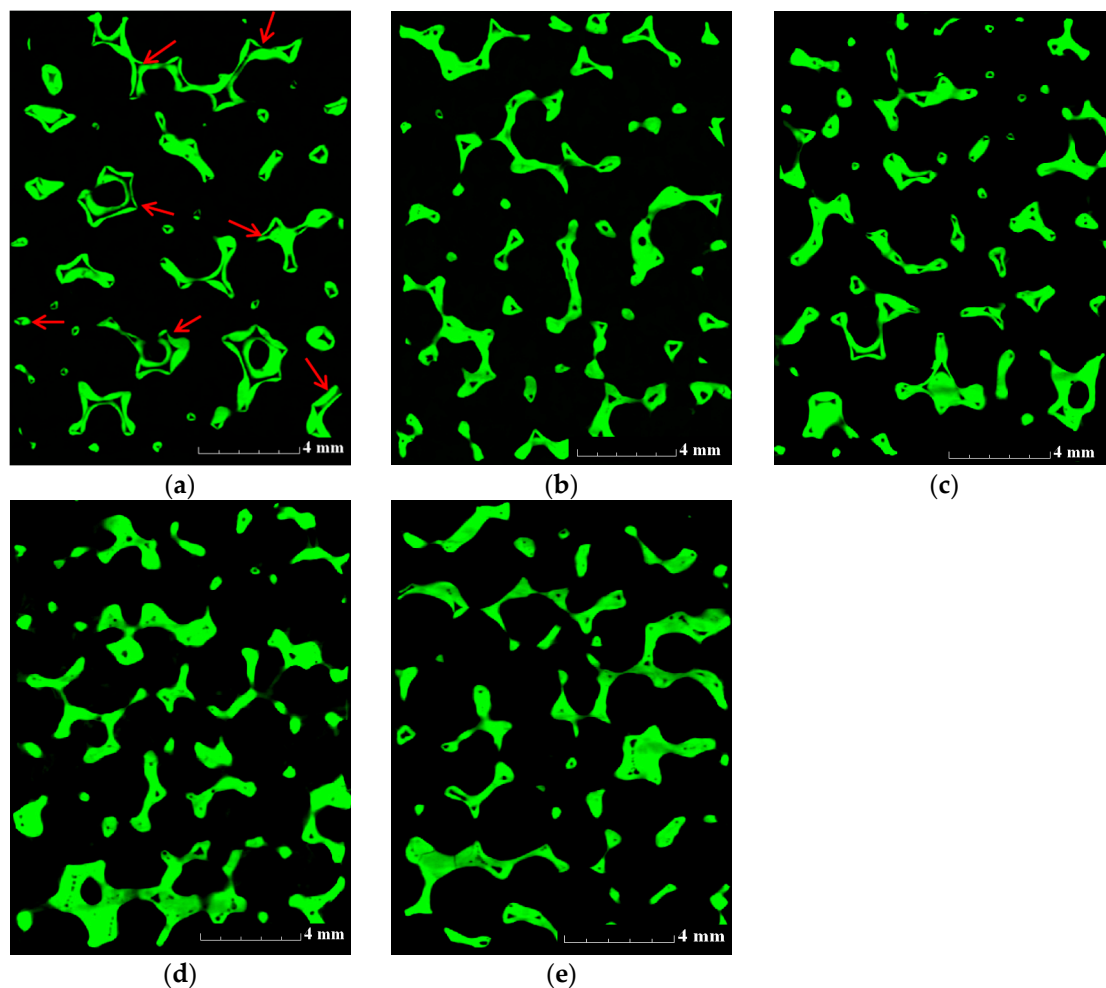

Figure 7. Cross-section images of ZTA foams from μ-CT 3D reconstruction: (**a**) ZTA20-80 pre-sintered at 1200 °C for 3 h; (**b**) ZTA20-50-10; (**c**) ZTA20-50-60; (**d**) ZTA20-60-10 and (**e**) ZTA20-60-60.

The compression strength of ZTA foams was markedly enhanced by immersion infiltration processing (Figure 8a). The highest improvement of compression strength is observed for ZTA20-60-60 (2.66 MPa, 2.5-fold of ZTA20-80), and the lowest improvement was for ZTA20-60-10 (2.09 MPa, 2.0-fold of ZTA20-80). However, the solid load of the immersion slurry and the dwelling time did not notably

influence the strength improvement, which is attributed to the filling of hollow struts by ZTA materials, which reduces the stress concentration at the sharp edges [41,42]. Additionally, eliminating the flaws and defects outside the strut surface also contributes to the strength increase, but it accounts only for a small fraction of it, as the initial strut surface of the starting ZTA foams was relatively smooth without a large number of severe flaws and defects. As listed in Table 1, the mean strut thickness of infiltrated foams remains almost the same as the original foams, which indicates that the strength improvements of ZTA PRCs is also not associated with the thickening of the struts.
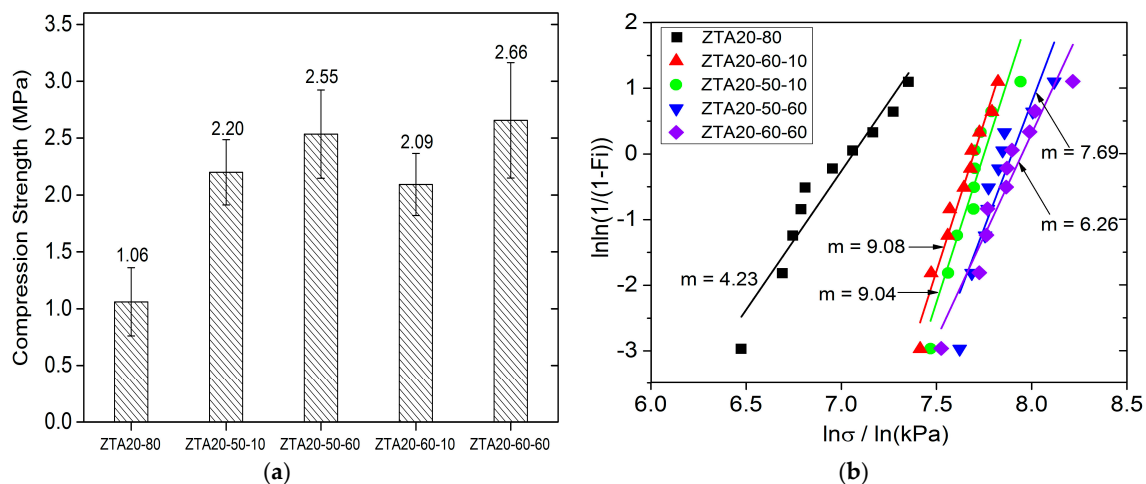

Figure 8. Compression tests for ZTA foams after infiltration: (**a**) the improvements of compression strength for ZTA foams after immersion infiltration (ZTA20-80 is the uninfiltrated starting material); and (**b**) the Weibull distribution plots of infiltrated ZTA foams.

Figure 8b demonstrates the Weibull distribution of the compression strength of ZTA foams after immersion infiltration processing. Clearly, the compressive values scatter in a very narrow range, and the Weibull modulus for ZTA foams is greatly improved. For the samples soaked for 10 min, they obtained Weibull moduli of 9.08 and 9.04, respectively, which are even more than two-fold the values of the original foams (m = 4.23). For the foams with the dwelling time of 60 min, even though their Weibull moduli of compressive values is lower than one of their counterparts of 10 min, they also achieved a high level, with the values of 7.69 and 6.26, respectively. The fulfillment of a high Weibull modulus means the immersion infiltration processing is quite an effective strategy to facilitate the mechanical stability of ZTA foams and is not restricted to alumina foams [18].

Figure 9 shows the density and porosity of ZTA foams after immersion infiltration. It can be observed that the density of ZTA foams experiences an increase from 0.43 g·cm^{-3} to around 0.55 g·cm^{-3}; correspondingly, the porosity of them decreases. However, the porosity of foams after the processing is still at a high level (above 86%), and taking the strength and Weibull modulus into account, ZTA foams possessing high strength, high porosity, and excellent stability were generated with the immersion infiltration strategy.
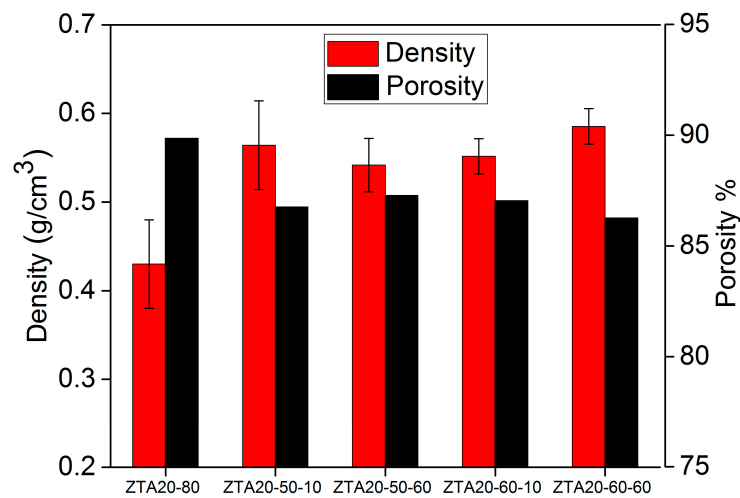
Figure 9. Density and porosity of ZTA foams after immersion infiltration (ZTA20-80 is the uninfiltrated starting material).

3.3. Improving the Strength of ZTA Foams by Recoating

As presented in Figure 10a,b, the weight gain, the porosity and compression strength of ZTA foams all show an almost linear dependence on the number of recoating cycles. The weight gain relative to the starting foam is about 50% for the first recoating cycle, and 250% after four recoating cycles. Correspondingly, the porosity decreases linearly from 89.9% to 58.5% as the number of recoating cycles increases. For two or fewer recoating cycles, the porosity of ZTA foams remains above 70%. The compression strength of recoated ZTA foams was significantly enhanced to 3.26 MPa (three-fold of ZTA20-80) and 5.61 MPa (five-fold of ZTA20-80) after one and two recoating cycles, respectively. The main reason for the strength improvements by recoating is the thickening of foam struts with the number of recoating cycles, as shown in Figure 10b. The mean strut thickness of the original foams is around 0.56 mm and, after two and four cycles, 0.95 mm and 1.41 mm, respectively. In addition, the elimination of surface flaws and defects also partly contributes to that. The compression strength was also evaluated with the Gibson-Ashby model [1] according to Equation (1), where σ_{cr}^* is the collapse stress of the foam; σ_{fs} is the modulus of rupture of the strut material, valued as 800 MPa [5]; C is a relation constant, equal to 0.2; p is the porosity of the foams. The predictions of the Gibson-Ashby model and our data are presented in Figure 10d. Our data are in good agreement with the Gibson-Ashby model and the compression strength decreases with an increasing porosity.

$$\frac{\sigma_{cr}^*}{\sigma_{fs}} = C(1-p)^{3/2} \tag{1}$$

The Weibull modulus of ZTA foams with recoating processing was also analyzed (Figure 10c). The Weibull modulus for samples ZTA-R2 and ZTA-R4 increase to 7.62 and 8.80, respectively, while the Weibull modulus for ZTA-R1 drops slightly to 4.04 compared to the value (4.23) of the base foams (ZTA20-80). Therefore, with a prerequisite of the cellular version for ZTA foams, recoating the green bodies of ZTA foams for two cycles is an appropriate processing setting in pursuit of high mechanical stability.
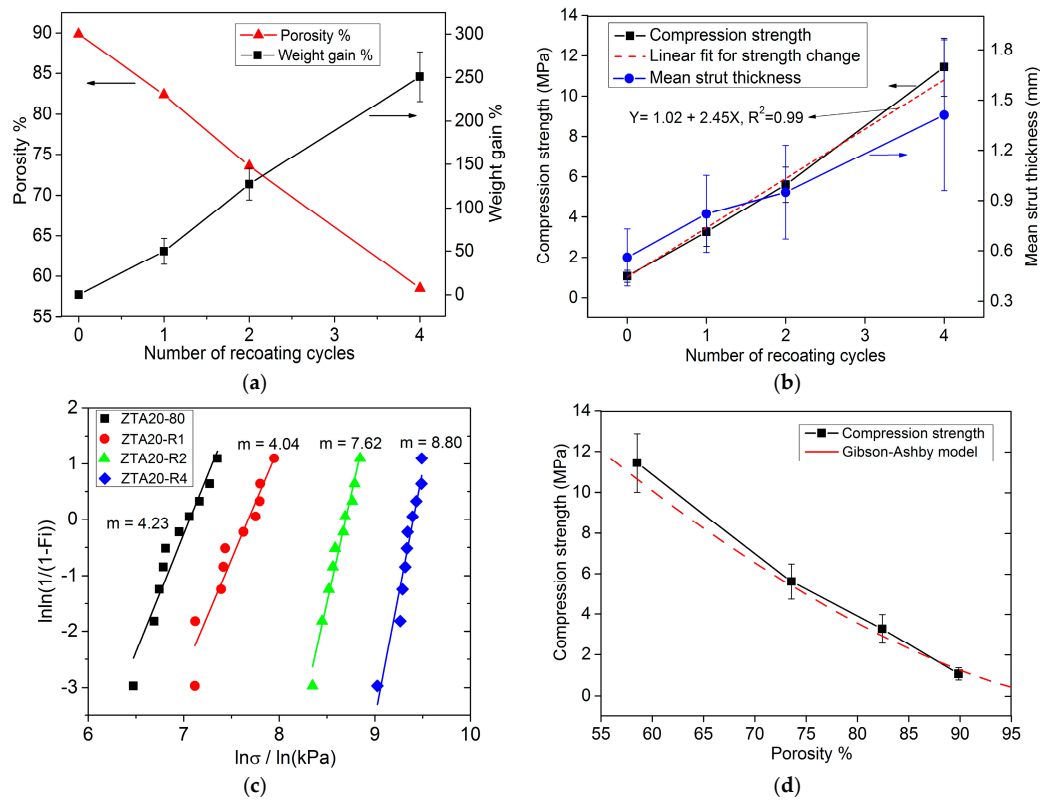
Figure 10. The recoating cycle dependence of the properties of ZTA foams: (**a**) the porosity and weight gain; (**b**) compression strength and mean strut thickness; (**c**) Weibull distribution plots of recoated ZTA foams and (**d**) the relation of porosity and compression strength compared with the Gibson-Ashby model.

The macrostructure of ZTA foams after recoating is shown in Figure 11. The strut thickness increases with recoating cycles, especially for the sample after four recoating cycles, in which the struts are extremely thick. The uniformity of ZTA foams also degrades after recoating treatment with some pores being blocked. In the sample recoated for four cycles, the interconnected pore space is severely reduced to about 50% of the foam volume (Figure 11d). However, for the foams recoated for one cycle (Figure 11b) and two cycles (Figure 11c), the original macrostructure with a high pore space fraction is observed. Taking the strength improvement and porosity drop into account, the one and two cycles of recoating are the best processing options to balance both parameters.
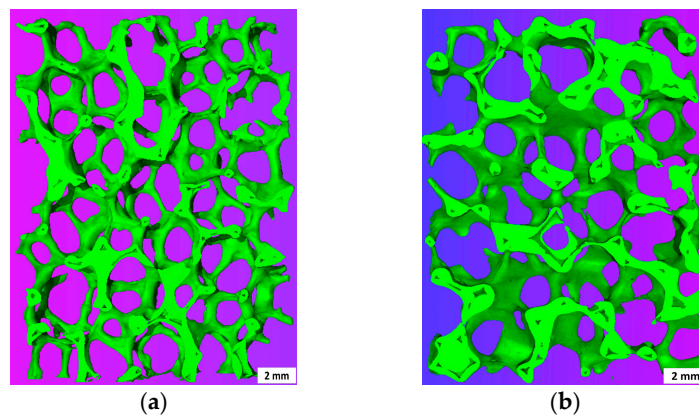

Figure 11. *Cont.*
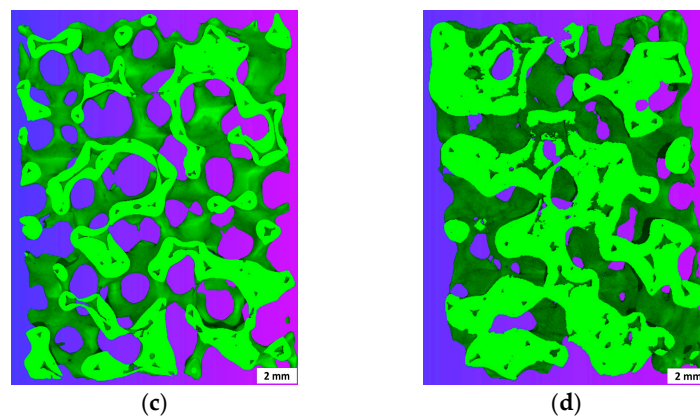
Figure 11. μ-CT 3D reconstruction of 3-mm thick slices from ZTA foams after recoating: (**a**) ZTA20-80; (**b**) ZTA20-R1; (**c**) ZTA20-R2 and (**d**) ZTA20-R4.

3.4. Comparison of Different Strengthening Methods

Several strategies have been proposed to strengthen ceramic foams, which are summarized in Figure 12. Without concern for the porosity, the recoating method is the most effective strengthening approach. By contrast, the infiltration approach can make moderate strength improvements, but with a much lower porosity drop. It is noteworthy that the immersion infiltration strategy proposed in the present work generates high strength improvements (about 1.5 MPa) associated with only a small reduction of total porosity of about 2–3%, so it is a good trade-off between mechanical strength and porosity.
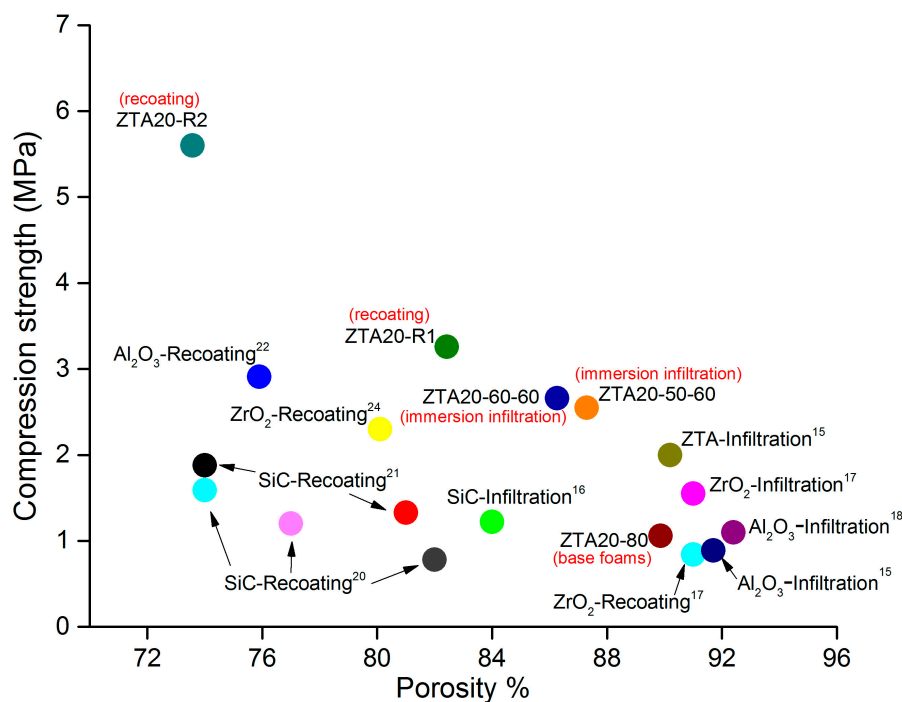

Figure 12. Comparison of reported infiltrated and recoated RPCs to the presented results.

4. Conclusions

The solid load of the slurry imposed a significant influence on the properties of the ZTA foams with regard to the density, porosity, and compression strength, whereby a higher solid load was associated by a lower sintering shrinkage and porosity, but a higher density and compressive strength. Immersion

infiltration was proven as an effective strategy to enhance the mechanical properties without a major change in porosity. Along with the simple equipment and operations, it can be applied to other RPCs as well. The application of the immersion infiltration is comparable to the recoating and, therefore, should be realizable in industrial processing. The recoating method greatly facilitates the strength of ZTA foams, and the recoating cycle dependence of foam properties shows a quite linear relation.

Author Contributions: For this work, Xiaodong Chen, Ulf Betke, Stefan Rannabauer, Gerrit Maximilian Söffker, and Michael Scheffler conceived and designed the experiments; Xiaodong Chen and Paul Clemens Peters performed the experiments; Xiaodong Chen, Ulf Betke, Stefan Rannabauer, and Michael Scheffler analyzed the data; Ulf Betke and Stefan Rannabauer contributed to the analysis equipment; and Xiaodong Chen wrote the paper.

Conflicts of Interest: The authors declare no conflict of interest.

References

1. Gibson, L.J.; Ashby, M.F. *Cellular Solids: Structure and Properties*, 2nd ed.; Cambridge University Press: London, UK, 1997; pp. 1–500.
2. Scheffler, M.; Colombo, P. *Cellular Ceramics: Structure, Manufacturing, Properties and Applications*; Weily-VCH: Weinheim, Germany, 2005; pp. 1–617.
3. Colombo, P. Conventional and novel processing methods for cellular ceramics. *Philos. Trans. A. Math. Phys. Eng. Sci.* **2006**, *364*, 109–124. [CrossRef] [PubMed]
4. Studart, A.R.; Gonzenbach, U.T.; Tervoort, E.; Gauckler, L.J. Processing routes to macroporous ceramics: A review. *J. Am. Ceram. Soc.* **2006**, *89*, 1771–1789. [CrossRef]
5. Wang, J.; Stevens, R. Review zirconia-toughened alumina (ZTA) ceramics. *J. Mater. Res.* **1989**, *24*, 3421–3440.
6. Hannink, R.H.J.; Kelly, P.M.; Muddle, B.C. Transformation toughening in zirconia-containing ceramics. *J. Am. Ceram. Soc.* **2000**, *87*, 461–487. [CrossRef]
7. Chevalier, J.; Gremillard, L.; Virkar, A.V.; Clarke, D.R. The tetragonal-monoclinic transformation in zirconia: Lessons learned and future trends. *J. Am. Ceram. Soc.* **2009**, *92*, 1901–1920. [CrossRef]
8. Hossen, M.; Chowdhury, F.Z.; Gafur, A.M.; Hakim, A.M.A. Structural and mechanical properties of zirconia toughened alumina (ZTA) composites. *Int. J. Eng. Res. Tec.* **2014**, *3*, 2128–2134.
9. Biotteau, D.K.; Zych, L.; Gremillard, L.; Chevalier, J. Effects of Ca-, Mg- and Si-doping on microstructures of alumina–zirconia composites. *J. Eur. Ceram. Soc.* **2012**, *32*, 2711–2721. [CrossRef]
10. Kern, F.; Palmero, P. Microstructure and mechanical properties of alumina 5 vol % zirconia nanocomposites prepared by powder coating and powder mixing routes. *Ceram. Int.* **2013**, *39*, 673–682. [CrossRef]
11. Sommer, F.; Walcher, H.; Kern, F.; Maetzig, M.; Gadow, R. Influence of feedstock preparation on ceramic injection molding and microstructural features of zirconia toughened alumina. *J. Eur. Ceram. Soc.* **2014**, *34*, 745–751. [CrossRef]
12. Nevarez-Rascon, A.; Aguilar-Elguezabal, A.; Orrantia, E.; Bocanegra-Bernal, M.H. Compressive strength, hardness and fracture toughness of Al_2O_3 whiskers reinforced ZTA and ATZ nanocomposites: Weibull analysis. *Int. J. Ref. Met. Hard Mater.* **2011**, *29*, 333–340. [CrossRef]
13. Azhar, A.Z.A.; Mohamad, H.; Ratnam, M.M.; Ahmad, Z.A. The effects of MgO addition on microstructure, mechanical properties and wear performance of zirconia-toughened alumina cutting inserts. *J. Alloys Compd.* **2010**, *497*, 316–320. [CrossRef]
14. Karl, S.; Somers, A.V. Method of Making Porous Ceramic Articles. U.S. Patent 3090094 A, 21 May 1963.
15. Vogt, U.F.; Gorbar, M.; Dimopoulos-Eggenschwiler, P.; Broenstrup, A.; Wagner, G.; Colombo, P. Improving the properties of ceramic foams by a vacuum infiltration process. *J. Eur. Ceram. Soc.* **2010**, *30*, 3005–3011. [CrossRef]
16. Liang, X.; Li, Y.; Liu, J.; Sang, S.; Chen, Y.; Li, B.; Aneziris, C.G. Fabrication of SiC reticulated porous ceramics with multi-layered struts for porous media combustion. *Ceram. Int.* **2016**, *42*, 13091–13097. [CrossRef]
17. Jun, I.K.; Kong, Y.M.; Lee, S.H.; Kim, H.E.; Kim, H.W.; Goretta, K.C. Reinforcement of a reticulated porous ceramic by a novel infiltration technique. *J. Am. Ceram. Soc.* **2006**, *89*, 2317–2319. [CrossRef]

18. Rannabauer, S.; Söffker, G.M.; Scheunemann, M.; Betke, U.; Scheffler, M. Increased mechanical stability and thermal conductivity of alumina reticulated porous ceramics (RPC) by nanoparticle infiltration processing. *Adv. Eng. Mater.* **2017**. [CrossRef]

19. Pu, X.; Liu, X.; Qiu, F.; Huang, L. Novel method to optimize the structure of reticulated porous ceramics. *J. Am. Ceram. Soc.* **2004**, *87*, 1392–1394. [CrossRef]

20. Yao, X.; Tan, S.; Huang, Z.; Jiang, D. Effect of recoating slurry viscosity on the properties of reticulated porous silicon carbide ceramics. *Ceram. Int.* **2006**, *32*, 137–142. [CrossRef]

21. Yao, X.; Yang, Y.; Liu, X.; Huang, Z. Effect of recoating slurry compositions on the microstructure and properties of SiC reticulated porous ceramics. *J. Eur. Ceram. Soc.* **2013**, *33*, 2909–2914. [CrossRef]

22. Voigt, C.; Jäckel, E.; Aneziris, C.G.; Hubálková, J. Investigations of reticulated porous alumina foam ceramics based on different coating techniques with the aid of μ-CT and statistical characteristics. *Ceram. Int.* **2013**, *39*, 2415–2422. [CrossRef]

23. Vogt, U.F.; Györfy, L.; Herzog, A.; Graule, T.; Plesch, G. Macroporous silicon carbide foams for porous burner applications and catalyst supports. *J. Phys. Chem. Solids* **2007**, *68*, 1234–1238. [CrossRef]

24. Herrera, A.M.; Martins de Oliveira, A.A.; Novaes de Oliveira, A.P.; Hotza, D. Processing and characterization of yttria-stabilized zirconia foams for high-temperature applications. *J. Ceram.* **2013**, *2013*, 1–8. [CrossRef]

25. Ren, F.; Zhai, G.; Ma, Z.; Volinsky, A.A.; Tian, B. Recoating slurry process effects on the SiC-based casting foam filter properties. *J. Ceram. Process. Res.* **2014**, *15*, 71–75.

26. Han, F.; Zhong, Z.; Yang, Y.; Wei, W.; Zhang, F.; Xing, W.; Fan, Y. High gas permeability of SiC porous ceramics reinforced by mullite fibers. *J. Eur. Ceram. Soc.* **2016**, *36*, 3909–3917. [CrossRef]

27. Yao, X.; Tan, S.; Huang, Z.; Dong, S.; Jiang, D. Growth mechanism of β-SiC nanowires in SiC reticulated porous ceramics. *Ceram. Int.* **2007**, *33*, 901–904. [CrossRef]

28. Washbourne, C. Catalyst Carriers. U.S. Patent 3972834 A, 3 August 1976.

29. Blome, C.J. Molten Metal Filter. U.S. Patent 4265659 A, 5 May 1981.

30. Brockmeyer, J.W.; Hendersonville, N.C. Ceramic Foam Filter and Aqueous Slurry for Making Same. U.S. Patent 4391918 A, 5 July 1983.

31. Pu, X.; Jia, L.; Zhang, D.; Su, C.; Liu, X. Surface treatment of templates for fabrication of reticulated porous ceramics. *J. Am. Ceram. Soc.* **2007**, *90*, 2998–3000. [CrossRef]

32. Jun, I.-K.; Koh, Y.-H.; Song, J.-H.; Lee, S.-H.; Kim, H.-E. Improved compressive strength of reticulated porous zirconia using carbon coated polymeric sponge as novel template. *Mater. Lett.* **2006**, *60*, 2507–2510. [CrossRef]

33. Ravaunt, F. Production of Porous Ceramic Materials. U.S. Patent 4004933 A, 25 January 1977.

34. Luyten, J.; Thijs, I.; Vandermeulen, W.; Mullens, S.; Wallaeys, B.; Mortelmans, R. Strong ceramic foams from polyurethane templates. *Adv. Appl. Ceram.* **2005**, *104*, 4–8. [CrossRef]

35. Paiva, A.; Sepulveda, P.; Pandolfelli, V. Processing and thermomechanical evaluation of fiber-reinforced alumina filters. *J. Mater. Sci.* **1999**, *34*, 2641–2649. [CrossRef]

36. Zhu, X.; Jiang, D.; Tan, S. Improvement in the strength of reticulated porous ceramics by vacuum degassing. *Mater. Lett.* **2001**, *51*, 363–367. [CrossRef]

37. Brown, D.D.; Green, J.D. Investigation of strut crack formation in open cell alumina ceramics. *J. Am. Ceram. Soc.* **1994**, *77*, 1467–1472. [CrossRef]

38. Betke, U.; Dalicho, S.; Rannabauer, S.; Lieb, A.; Scheffler, F.; Scheffler, M. Impact of slurry composition on properties of cellular alumina: A computed tomographic study. *Adv. Eng. Mater.* **2017**. [CrossRef]

39. Nikolay, D.; Kollenberg, W.; Deller, K.; Oswald, M.; Tontrup, C. Manufacturing and properties of ZTA-ceramics with nanoscaled ZrO_2. *Ceram. Forum Int.* **2006**, *83*, 35–37.

40. Lange, F.F.; Hirlinger, M.M. Hindrance of grain growth in Al_2O_3 by ZrO_2 inclusions. *J. Am. Ceram. Soc.* **1984**, *67*, 164–168. [CrossRef]

41. Brezny, R.; Green, J.D.; Dam, Q.C. Evaluation of strut strength in open-cell ceramics. *J. Am. Ceram. Soc.* **1989**, *72*, 885–889. [CrossRef]

42. Dam, Q.C.; Brezny, R.; Green, J.D. Compressive behavior and deformation-mode map of an open cell alumina. *J. Mater. Res.* **1990**, *5*, 163–171. [CrossRef]